1

Theoretical Studies and Tailored Computer Simulations in Self-Assembling Systems: A General Aspect

Zihan Huang and Li-Tang Yan

Key Laboratory of Advanced Materials (MOE), Department of Chemical Engineering, Tsinghua University, Beijing, China

1.1 Introduction

Self-assembly—a governing principle by which materials form—is the autonomous organization of matter into ordered arrangements [1, 2]. It is typically associated with thermodynamic equilibrium, the organized structures being characterized by a minimum in the system's free energy, although this definition is too broad. Self-assembling processes are ubiquitous in nature, ranging, for example, from the opalescent inner surface of the abalone shell to the internal compartments of a living cell [3]. By these processes, nanoparticles or other discrete components spontaneously organize due to direct specific interactions and/or indirectly, through their environment. Self-assembly is one of the few practical strategies for making ensembles of nanostructures. It will therefore be an essential part of nanotechnology. Self-assembly is also common to many dynamic, multicomponent systems, from smart materials and self-healing structures to netted sensors and computer networks. In the world of biology, living cells self-assemble, and understanding life will therefore require understanding self-assembly. The cell also offers countless examples of functional self-assembly that stimulate the design of non-living systems [4, 5].

Self-assembly reflects information coded (as shape, surface properties, charge, polarizability, magnetic dipole, mass, etc.) in individual components; these characters determine the interaction among them. The design of building blocks that organize themselves into desired structure and functions is the key to applications of self-assembly [2]. Much of materials science and soft condensed-matter physics in the past century involved the study of self-assembly of fundamental building blocks (typically atoms, molecules, macromolecules, and colloidal particles) into bulk thermodynamic phases [6]. Today, the extent to which these building blocks can be engineered has undergone a quantum leap. Tailor-made, submicrometer particles will be the building blocks of a new generation of nanostructured materials with unique physical properties [7–11]. These new building blocks will be the "atoms" and "molecules" of tomorrow's materials, self-assembling into novel structures made possible solely by their unique design [2]. For example, patchy particles consisting of various

Self-Assembling Systems: Theory and Simulation, First Edition. Edited by Li-Tang Yan.

compartments of different chemistry or polarity are ideal building blocks of potentially complex shapes with competing interactions that expand the range of self-assembled structures beyond those exhibited by traditional amphiphiles such as surfactants and block copolymers [9]. By controlling the placement of "sticky" patches on the particles, assemblies can be made that mimic atomic bonding in molecules [8]. This greatly expands the range of structures that can be assembled from small components. Extension of the principles to particles of alternative compositions (such as those made from noble metals, semiconductors or oxides) will allow optical, electronic and catalytic materials to be coupled in previously impossible architectures that have potentially new emergent properties. Playing tricks with designer "atoms" also includes the shape of the building blocks [12]. For instance, the local curvature of dumbbell-shaped nanoparticles can be harnessed to control the ionization state of a molecular layer adsorbed on their surfaces and the self-assembly patterns of the particles [13].

Understanding the relation between building blocks and their assemblies is essential for materials design because physical properties depend intimately on structure, which however poses many challenges if considering complex thermodynamic and kinetic behaviors involved in the assembling processes. Indeed, a priori prediction of hierarchically assembled structures from a desired building block requires an in-depth understanding of the delicate balance between entropic and enthalpic interactions [14–17]. Central to this issue is exploring entropy-driven structural organization, because entropy keeps springing non-intuitive findings in the manipulation of the self-assembly of nanoparticles and the structural formation of soft matter systems [14]. On the other hand, directed self-assembly using a template or an external field may also give rise to novel ordered non-equilibrium structures, free from the constraints of entropy maximization, and hence these systems can "reside" in a state of local equilibrium within the global free energy with low entropy states often characterized by complex spatial or coherent spatiotemporal organization [18]. In this case, identifying the possible structures at metastable states is important for controlling the formation of structures or patterns. Not surprisingly, many advances have been made in theoretical models and simulation approaches to predict and analyze structures, dynamics and properties of self-assembling systems; computer simulations offer a unique approach to identify and separate individual contributions to the phenomenon or process of interest [19, 20].

However, the theoretical and computational research of self-assembling systems is far from trivial. These many-body systems cover variations in relevant time and length scales over many orders of magnitude. The assembled structures and macroscopic properties of materials are ultimately to be deduced from the dynamics of the microscopic, molecular level, implicating a lot of demand for new simulation techniques and theoretical approaches. From the computational point of view, the key is to develop methods capable of reaching time and length scales much larger than those accessible by brute force computer simulations on the atomic level [21]. The feat is not a simple one, since it requires a major effort over a wide range of activities, including the development of coarse graining techniques, novel simulation methods and ways to link the different regimes to each other. Even with these challenges, theory and simulations have proven invaluable and indispensable in studies of self-assembling systems, including applications in numerous directions such as development and examination of new principles, predictive science and computer design of complex building blocks, suggesting guidelines of programmable assembly, and exploring entropy interaction in various

assembling systems, etc. The purpose of this chapter is therefore to introduce the general aspects of the development and applications of theoretical approaches and computational modeling in self assembling systems, focusing on basic and emerging principles.

1.2 Emerging Self-Assembling Principles

1.2.1 Predictive Science and Rational Design of Complex Building Blocks

Predicting structure from the attributes of a material's building blocks remains a challenge and the central goal for materials science. Here we introduce the rational design and predictive science of two emerging and important building blocks for superstructure construction through self-assembly, that is, polyhedral particles and particles that can self-assemble into helical structures with chirality.

At present, a major focus in material science is to engineer particles with anisotropic shapes and interaction fields that can be self-assembled into complex target structures [1, 2]. Assemblies of anisotropic particles undergo order – disorder transitions involving changes in both translational and rotational degrees of freedom and can lead to phases with partial structural order or "mesophases" [22, 23] such as crystals, plastic crystals and liquid crystals. These ordered assemblies have distinctive electronic, optical and dynamical properties and are highly desirable for fabrication of advanced electronic, photonic and rheological devices [24]. Although numerous theoretical [25, 26] and experimental [27, 28] studies on mesophase behavior of particles with anisotropic shapes have been reported, a roadmap marking out the most probable mesophases that could be formed by constituent particles with particular geometrical features remains incomplete. Exploring such relations will translate into a deeper understanding of the phase behavior of colloidal systems with different particle shapes. The simulation prediction of a dodecagonal quasicrystal with tetrahedra demonstrated the unexpected complexity that could be achieved for particles solely with hard interactions [29]. Escobedo and Agarwal [30] carried out detailed Monte Carlo simulations of six convex space-filling polyhedrons to demonstrate that translational and orientational excluded-volume fields encoded in particles with anisotropic shapes can lead to purely entropy-driven assembly of morphologies with specific order and symmetry. Their simulations reveal the formation of various new liquid-crystalline and plastic-crystalline phases at intermediate volume fractions. They further propose simple guidelines for predicting phase behavior of polyhedral particles: high rotational symmetry is in general conducive to mesophase formation, with low anisotropy favoring plastic-solid behavior and intermediate anisotropy (or high uniaxial anisotropy) favoring liquid-crystalline behavior.

Recently, a more refined structure prediction of polyhedral particles has been attained by Glotzer et al. [31] through investigating 145 convex polyhedra whose assembly arises solely from their anisotropic shape. Their simulations demonstrate that from simple measures of particle shape and local order in the fluid, the assembly of a given shape into a liquid crystal, plastic crystal or crystal can be predicted. Two important shape parameters that were revealed to predict the general category of ordered structure are the coordination number and the isoperimetric quotient (Figure 1.1). Although still unable to predict a specific structure, their results provide an important step toward a predictive

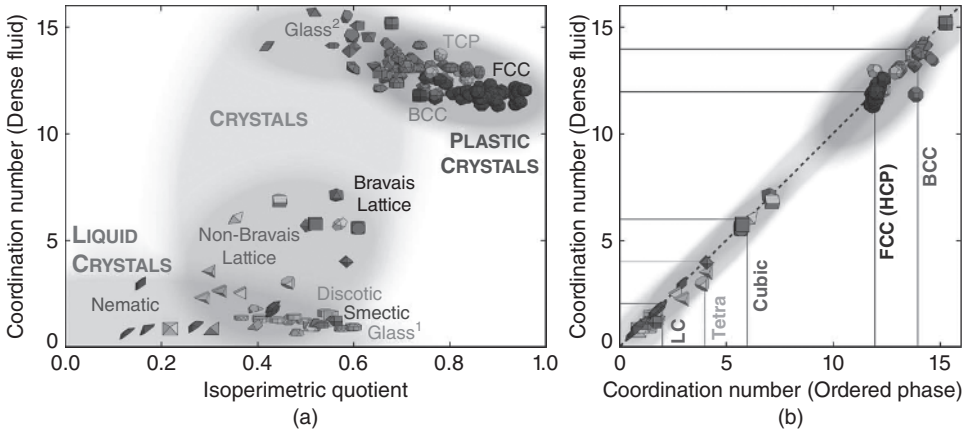

Figure 1.1 (a) The coordination number in the fluid phase, CN_f, is correlated to the isoperimetric quotient (*IQ*) of the polyhedron. Here, *IQ* is a scalar parameter for the sphericity of the shape and coordination number is a measure of the degree of local order. Data points are drawn as small polyhedra, which are grouped according to the assemblies they form. (b) Polyhedra have, in most cases, nearly identical coordination numbers in the ordered phase (CN_o) and the fluid phase (CN_f) close to the ordering transition. Because of this strong correlation, combining CN_f and *IQ* allows for prediction of the assembly category expected for most cases. This figure is reproduced from Ref. [31]. Copyright permission from American Association for the Advancement of Science (2012). *(See insert for color representation of the figure.)*.

science of nanoparticle and colloidal assembly, which will be necessary to guide experiments with families of polyhedrally shaped particles that are now becoming available.

Rational design of building blocks for self-assembly can be significantly facilitated if the final structure can be predicted as a function of the building block parameters [30–33]. The interaction fields and anisotropic shapes encoded in the building blocks allow potential approaches for such a prediction. However, considering the complex energy landscape and kinetic pathway, the predictive science of sophisticated supracolloidal structures remains a key challenge. In particular, although numerous studies on the predictive self-assembly of anisotropic particles have been reported [30, 31], a priori prediction of helical supracolloidal structures from rationally designed building blocks still lacks a general roadmap and has yet to be demonstrated. Helical structure represents the principal element responsible for the property of chirality. Control over chirality at nano- and mesoscales is rapidly becoming a goal of great scientific interest because such unique architectures will allow optical, plasmonic and catalysis materials to have distinctively emergent properties [34–36]. This aspect is particularly relevant for photonic applications [37], where the optical properties are significantly influenced by the periodically arranged unit cells. Molecular scaffolds such as DNA origami can enable the high-yield production of superstructures that contain nanoparticles arranged in nanometer-scale helices [38]. However, large-scale fabrication of these scaffolds poses a significant hurdle for many practical applications.

The notion of a directional interaction field encoded by the surface patches suggests that patchy particles can be used to generate supracolloidal helices without fixed templates that offer limited controllability and may penalize the properties of particle assemblies [39, 40]. However, the ability to design and control supracolloidal helices

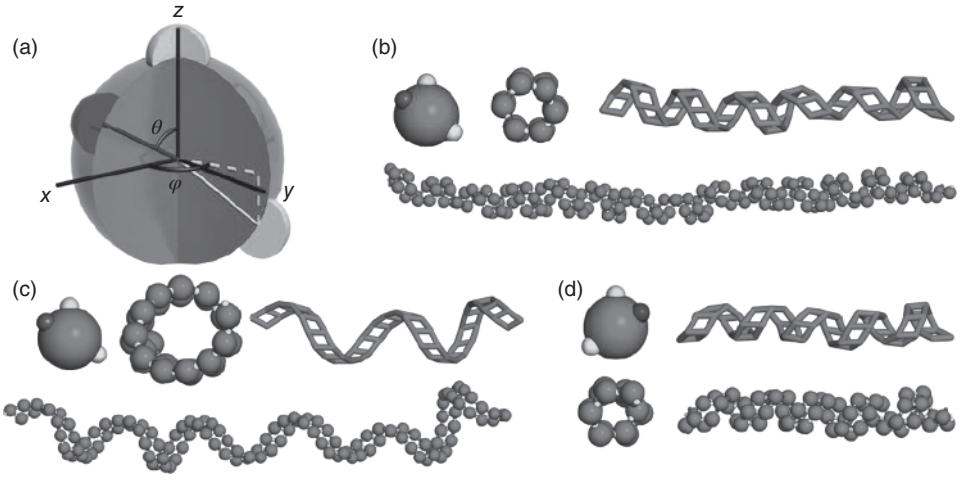

Figure 1.2 Tunable helical supracolloidal structures from a facile particle model. (a) Cartoon of patchy particle model used in the simulations. The top patch is a self-complementary patch while the other two patches are a pair of complementary patches. The relative directions of these patches are determined by angles θ and φ. (b) Right-handed double-stranded helix formed from patchy particles with patch direction of $\theta = 60°$ and $\varphi = 120°$. (c) Right-handed double-stranded helix with larger pitch and radius than those in (b), where the parameters are set as $\theta = 60°$, $\varphi = 150°$. (d) Left-handed double-stranded helix formed from patchy particles with patch direction of $\theta = 60°$ and $\varphi = -120°$. In (b)–(d), the building blocks and the top and side views of the helically supracolloidal structures and their geometrical representation are shown. This figure is reproduced from Ref. 41.Copyright Permission from Nature Publishing Group (2014).

assembled from patchy particles or colloids is limited by the absence of a general prediction principle. Challenges include exploring a facile design rule of patchy particles for helical self-assembly and further establishing a critical prediction principle for such supracolloidal architectures. Recently, inspired by biological helices, Guo et al. [41] showed that the rational design of patchy arrangement and interaction can drive patchy particles to self-assemble into biomolecular mimetic supracolloidal helices. They further derived a facile design rule for encoding the target supracolloidal helices, thus opening the doors to the predictive science of these supracolloidal architectures (Figure 1.2). It is also found that kinetics and reaction pathway during the formation of supracolloidal helices offer a unique way to study supramolecular polymerization, and that well-controlled supracolloidal helices can exhibit tailorable circular dichroism effects at visible wavelengths.

1.2.2 Entropy-Driven Ordering and Self-Assembly

Precise control of self-assembled structures remains a challenge because the structural architectures are governed by an intricate balance of entropic and enthalpic interactions. Central to this issue is exploring entropy-driven structural organization because entropy keeps springing non-intuitive findings in the manipulation of the self-assembly and the structural formation of soft matter systems [14–16, 42]. In fact, understanding entropic contributions to ordering transitions is essential for the design of self-assembling systems with hierarchical structures. Various unexpected structures can

form by self-assembly of tailor-made building blocks, and these can be designed so that such structures increase the entropy of the system [43–45]. Indeed, over the past few decades examples have been highlighted in which entropic interactions are exploited to direct self-assemblies, such as self-assembly of complex colloids, shape-entropy mediated particle assembly, hierarchical self-assembly in polymer nanocomposites, etc. In this section, we briefly summarize the advancement of these emerging topics as follow.

Entropy can be a subtle and elusive concept. Although in some sense it is the quantification of disorder, it has long been known that for hard colloidal spheres at high density an ordered crystal has higher entropy than a disordered fluid [46, 47]. Yet the formation of a crystal seems to be at odds with the widespread notion of entropy as a measure of disorder. Actually, this would only be possible if the entropy of the ordered phase were higher than that of the disordered phase at the same density and temperature [14]. In the system of densely packed hard colloidal spheres, the entropy loss caused by collective ordering of the mean atomic positions is more than compensated by the fact that each particle has more space to explore. Thus, the colloidal spheres must crystallize [into hexagonal close-packed or face-centered cubic lattices in three dimensions, and the hexagonal lattice in two dimensions (2D)] to gain accessible volume and thus entropy.

With patchy particles, however, this argument is partially reversed. Granick et al. [48] show that, through decoration of the particle surfaces with a simple pattern of hydrophobic domains, triblock Janus colloidal spheres can be induced to self-assemble into an open kagome structure, contrasting with previously known close-packed periodic arrangements of spheres. In this case, a crucial new factor is the "rotational rattle room," defined by the solid angle that each particle can rotate before any of its sticky patches lose contact with those of its neighbors (Figure 1.3a) [15]. A lost contact would represent a "broken bond," which is effectively forbidden by its relatively high energy penalty. Therefore, the rotational entropy of a patchy particle clearly depends on its environment, in contrast to what occurs for non-patchy hard spheres, which can always undergo complete rotation and for which entropy per particle is always a constant. Recently, Mao et al. [49] showed that under well-motivated limiting assumptions the rotational-entropy contribution is calculable analytically. They constructed an effective description of the interactions in a system of patchy particles with fluctuating lattice positions, and compared it with experimental data on the mode structure of lattice vibrations for triblock Janus spheres. Their calculations determined that in two dimensions the kagome lattice is more stable than the close-packed hexagonal lattice. Both lattices have four bonds per particle and thus the same energy, but at close packing the latter has two additional non-bonded contacts (Figure 1.3b). In a hexagonal crystal of the same density as the kagome lattice (whose maximum density is lower), patchy particles have more room to rattle translationally, but the combined entropy of rotation and vibration is reduced. For densities that are not too high, the latter effect dominates, and the kagome lattice is stabilized.

If the particles are non-spherical, the optimal packing geometry is not always clear. The systematic study of families of idealized colloidal and nanoscale systems by computer simulation has produced overwhelming evidence that shape is implicated in the self-assembly of model systems of particles [50, 51]. In these model systems, the only intrinsic forces between particles are steric, and the entropic effects of shape (which we term "shape entropy") can be isolated. Damasceno et al. [31] have recently shown that arbitrarily shaped hard polyhedra display considerable predictability in their dense

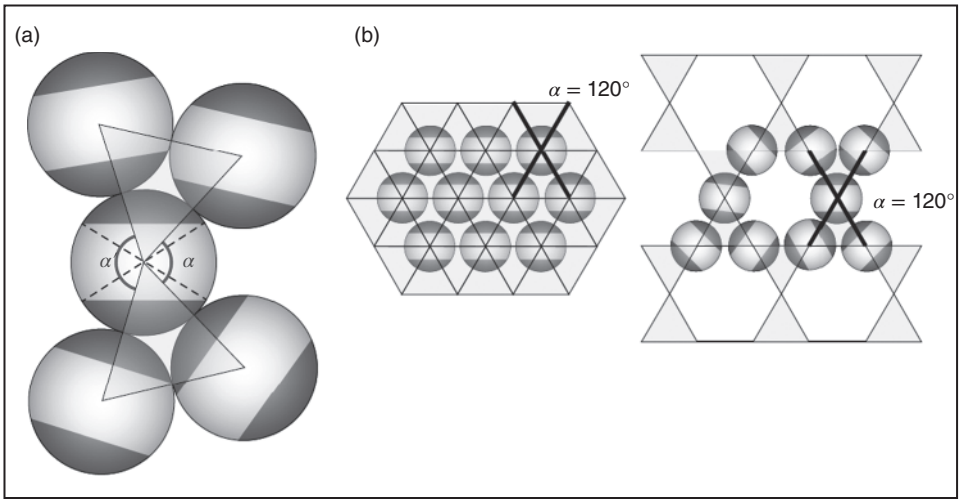

Figure 1.3 The rotational "rattle room" of patchy colloids. (a) Bonded contacts between triblock Janus spheres are maintained as long as the edges of the overlaid triangles cross the attractive dark gray patches. For a fixed particle configuration, the angular excursions that a particle can make without breaking any of its four contacts are independent of the corresponding excursions of neighboring particles. In two dimensions such a rotational entropy can therefore be calculated one particle at a time, and depends only on the bond angles α and α'. (b) The hexagonal (left) and kagome (right) lattices have the same number of bonded contacts and thus the same energy per particle. However, for moderate densities, particles in a kagome lattice have less room to rattle by translation, yet more entropy from rotational and vibrational motions, than particles in a hexagonal lattice at the same density. The latter effect dominates, which favors the formation of the kagome crystal over the hexagonal. This figure is reproduced from Ref. [15]. Copyright permission from Nature Publishing Group (2013).

packing arrangements. Depending on their shape, some polyhedra will form ordered crystals, while others form liquid crystals, "plastic" crystals in which the particles rotate freely, or disordered glasses. The entropic forces promoting the dense phases here heed details of particle shape: in particular, there is often a propensity for particles to sit face to face with facets aligned, creating directional preferences that can lead to ordered self-assembly. However, the origin and strength of these forces are unclear.

Using computer simulations of polyhedral packings, Anders et al. [52] clarify the concept of a shape-dependent directional entropic force, showing that it can be given a rigorous description based on the role of shape and faceting in maximizing the entropy of dense packings. As such, the force is an emergent property of local particle configurations, and it typically manifests itself for polyhedra as a repulsion between corners and an attraction between faces. For these systems the force is typically of the order of a few kT (where k is Boltzmann's constant and T is temperature), making it comparable to van der Waals and depletion forces.

Another common example of entropy-driven self-assembly is polymer nanocomposite in which the mixing of polymers and nanoparticles is opening pathways for engineering flexible composites that exhibit advantageous electrical, optical or mechanical properties [16, 17, 53]. One typical system is diblock copolymer/nanoparticle mixtures where the microphase separation of the copolymer can direct the spatial

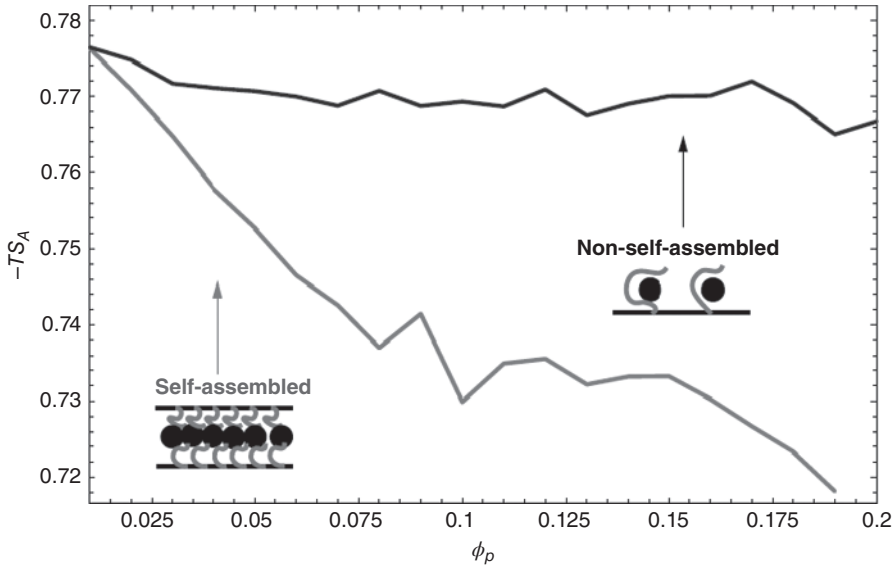

Figure 1.4 *A*-block entropic free energy contribution $-TS_A$ (where S_A is the conformational entropy of the *A* block) per polymer chain, for large particles ($R = 0.3R_0$, gray curve) and small particles ($R = 0.15R_0$, black curve), as a function of ϕ_p. This figure is reproduced from Ref. [56]. Permission from American Association for the Advancement of Science (2001).

distribution of nanoparticles and thereby tailor the properties of the composite [54, 55]. The optical performance of composites, for example, is highly sensitive to the specific location of the particles within the matrix, and the microphase separation of block copolymers can be used to great advantage. However, block copolymers do not simply "template" the arrangement of the nanoparticles. Because the nanoparticles are solids, the polymer chains must stretch around these obstacles, causing a loss in conformational entropy that increases with particle radius. In the absence of specific interactions, larger nanoparticles are expelled from the bulk of the copolymers, whereas smaller particles are not (Figure 1.4). This significantly affects the spatial distribution of nanoparticles within homopolymers and block copolymers and the hierarchical structure of particle-filled systems. Using a combination of self-consistent field- and density-functional theories, Thompson et al. [56] predicted that larger *A*-like particles (i.e., particles that are compatible with the *A* blocks of *AB* copolymers) localize at the center of the *A* microdomains, whereas smaller particles are more uniformly dispersed within a specific microdomain.

The observations above imply that the spatial distribution of nanoparticles in the microphase-separated morphologies can be controlled by tailoring the nanoparticle ligands (i.e., enthalpic effects) and the size of the nanoparticles relative to the radius of gyration of the polymer (i.e., entropic effects). For example, by blending *A*-like nanoparticles of different sizes with symmetric *AB* diblocks, one can fashion gradient materials within the *A* lamellae, where the largest particles are localized in the center, bordered by the next larger particles, which in turn are neighbored by smaller particles.

The entropic penalty associated with chain stretching around particles can also be harnessed to tailor the precisely interfacial organization of Janus nanoparticles in

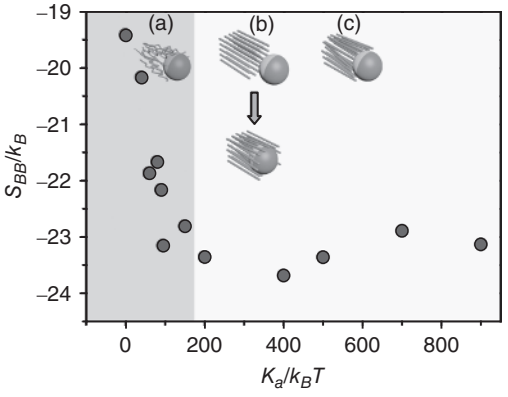

Figure 1.5 The K_a dependence of the excess entropy per bead, S_{BB}, calculated from the pair correlation function between *B*-block beads. The inset diagrams (a)–(c) show the position of Janus nanoparticles and the organization of the stiff *B* blocks around them in response to the increase of the chain stiffness. This figure is reproduced from Ref. [59]. Copyright permission from American Chemical Society (2015).

the scaffold of block copolymers [57–59]. For example, by combining coarse-grained molecular dynamics and a finite difference time domain technique, Dong et al. [59] report entropy-mediated precise interfacial organization of Janus nanoparticles in flexible–semiflexible block copolymers and the resulting optical properties of this heterogeneous material. They find that the stiffness of the semiflexible block can regulate the off-center distribution of symmetric Janus nanoparticles with respect to the phase interface, featured by a roughly 35% deviation from the interface to the utmost extent. The results reveal how entropic and enthalpic effects in this multiphase material contribute to the self-assembled morphologies and, in particular, can lead to entropically driven spatial transition of interfacial nanostructures (Figure 1.5). This might be the very first simulation study to capture the chain stiffness-dependent spatial transition in the interfacial assembly of nanoparticles, and thereby enables applications of chain stiffness in precise control over the interfacial assembly of nanoparticles in polymer scaffolds.

The entropic repulsion between tethered Janus nanoparticles at fluid interfaces can template the mixing of otherwise incompatible nanoparticles, toward perfect mixing of binary nanoparticles at single-nanoparticle level [60, 61]. Indeed, by means of computer simulations, Liu et al. [60] show novel mechanomutable nanocomposites designed by binary mixtures of tethered Janus nanoparticles at the interface of a binary fluid mixture under mechanical pressure. The nanoparticle organization in the systems exhibits a reversible transition between the random state and the long-ranged intercalation state that can be effectively controlled by various structural parameters of the tethered chains and the applied pressure (Figure 1.6). The dynamics mechanism of the transition is explored by examining the detailed trajectories of the interfacial nanoparticles during their 2D diffusion. The origin driving the collective organization of the binary Janus nanoparticles at the fluid–fluid interface is explained by combining computer simulations and theoretical analysis, revealing that both the conformational entropy effect of the tethered chains and sufficient tether disparity dominate the collective nanoparticle organization in the mechanical response behavior. The attractive feature of the procedure proposed by this work is that the interfacial nanostructures are tuned simply by pressing an accessible system containing binary tethered Janus particles in a binary fluid. The motif and findings described in this letter thereby suggest a facile route to create well-defined, responsive and flexible nanopatterns formed by multicomponent

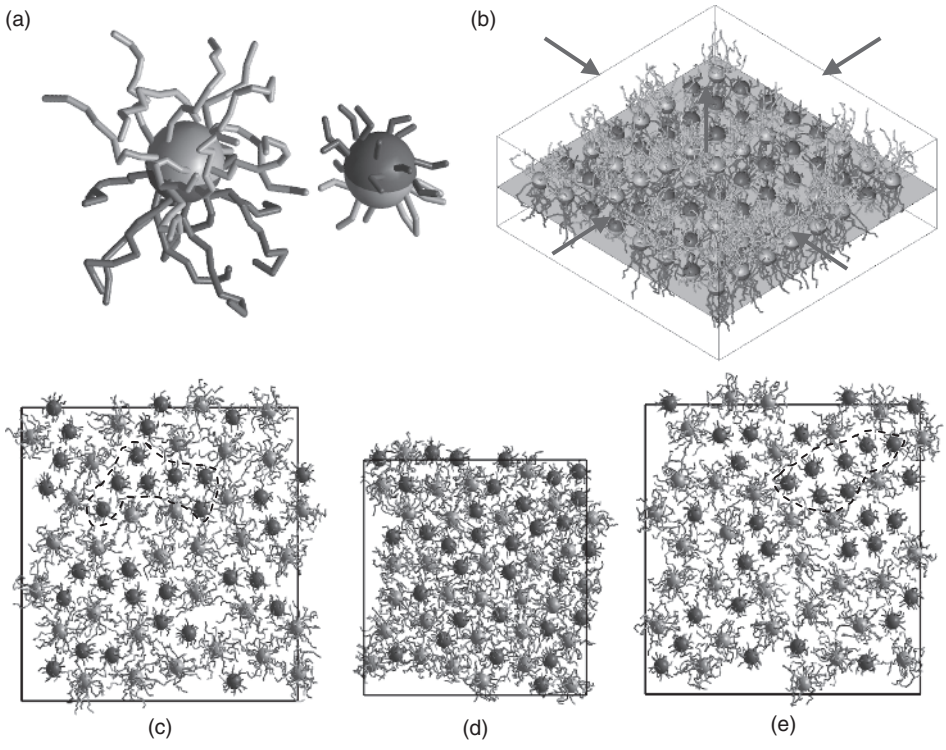

Figure 1.6 (a) Janus nanoparticles tethered with long and short ligand chains. (b) The random arrangement of nanoparticles at the fluid interface for the initial simulations. The gray plane surface represents the fluid interface whereas the fluid beads are not shown for clarity. The arrows indicate the lateral and vertical changes of the simulation box while applying mechanical pressure. (c)–(e) Top-view snapshots of the interfacial nanoparticle patterns where $S = S_0$ (c), $S = 0.64S_0$ (d) and $S = S_0$ (e). The dashed circles in (c) and (e) highlight the phase domains of the same nanoparticle component. This figure is reproduced from Ref. [60]. Copyright permission from American Chemical Society (2014).

nanoparticles in the interface of wide fluid mixtures, and consequently lead to a class of interface-reactive nanocomposites toward technologically important materials and devices.

1.2.3 Programmable Self-Assembly

Programmable self-assembly is an emerging and important concept for future materials fabrication toward precisely controlled structures and optimized properties. For more details of this concept please refer to a recent review by Cademartiri et al. [62]. Here we briefly summarize it and further introduce the theoretical aspect of the relative researches. The programmed assembly of structures from their components requires information [63, 64]—that is, instructions or guidance that direct the reproducible formation of a particular structure from myriad possibilities (Figure 1.7). Such "assembly information" must specify the location and connectivity of the building blocks within the assembled structure and, often, the order and manner in which they are added to it. The information encoded within the building blocks determines the

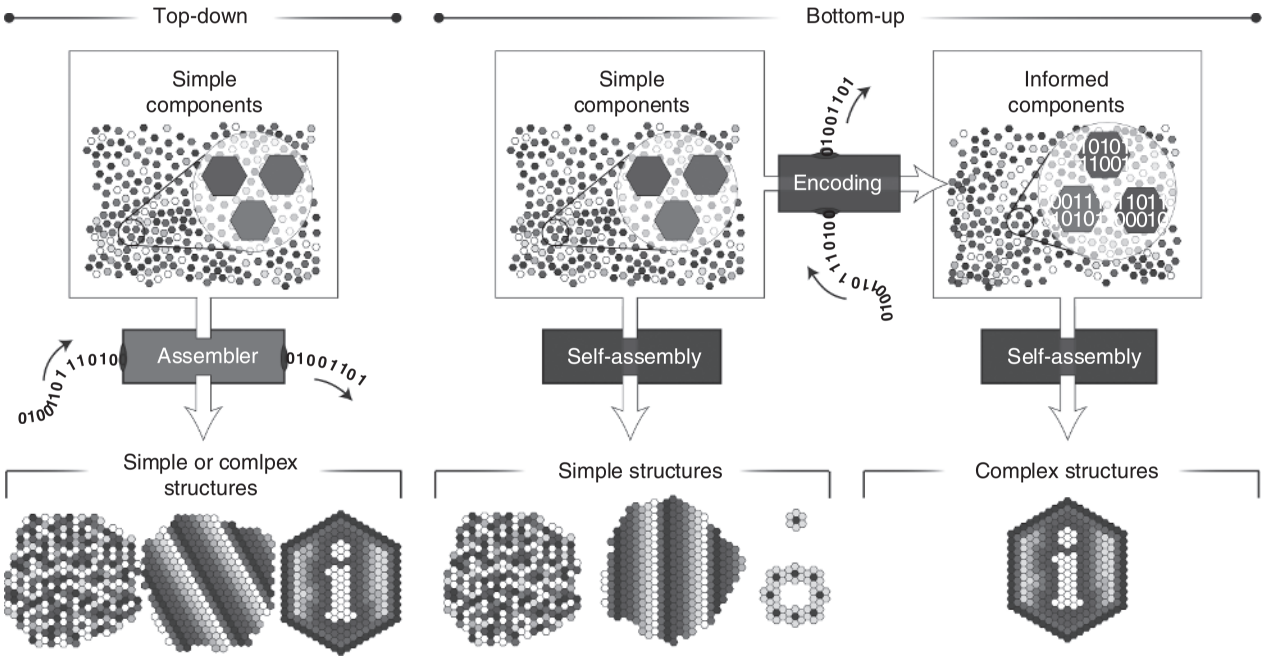

Figure 1.7 The role of information in top-down manufacturing and bottom-up self-assembly. Top-down manufacturing assembles simple building blocks into complex objects by using assemblers. This approach has been the standard strategy for manufacturing, but becomes increasingly difficult at the molecular and nanoscale. By contrast, the bottom-up self-assembly of simple (high-symmetry) components invariably leads to simple structures. The self-assembly of complex structures requires information-rich building blocks (informed components). This figure is reproduced from Ref. [62]. Copyright permission from Nature Publishing Group (2015).

complexity of the final structure [65], which at equilibrium minimizes the system's free energy and is determined by the accessible configurations and their respective energies. In this context, assembly information is encoded into the building blocks in two formats: constraints, which determine the accessible configurations, and interactions, which determine their energy [62].

DNA may be the only practical chemical system that can produce the large numbers of distinct and highly selective interactions preferred by programmable self-assembly [62]. Interactions based on DNA hybridization are well suited for this approach because of the large number of possible interactions, their high specificity and their tunable strength, typically achieved by varying the number of bases in the "sticky ends" of the DNA strands. Early examples of DNA-based interactions between nanoparticles constructed mostly dimers and trimers [66, 67], and have since been extended to achieve the reliable and programmable formation of nanocrystal superlattices [68, 69] and well-defined clusters [70, 71]. In this approach, colloidal building blocks present multiple types of single-stranded DNA on their surface and organize to form structures that maximize DNA hybridization [69]. Particle geometry can also modify both the strength and directionality of attractive surface forces. For example, two cubic particles coated with complementary DNA linkers will bind face to face to maximize DNA hybridization [72]. Recent advances in colloidal synthesis offer trivalent and tetravalent particles that enable directional bonding via specific DNA-based linkers [8]. These particles allow the programmed assembly of finite structures specified by assembly information encoded within selective DNA-based interactions, well-defined surface patches and steric constraints due to particle shape and size.

Theoretical analysis and simulations have played an important role in understanding the process and predicting the formed structures of programmable self-assembly. The results have not only confirmed the experimental results but also stimulate the experiments by providing new predictions.

From the theoretical point of view, the first analytical model was proposed by Tkachenko [73] in 2002, who obtained a phase diagram as a function of two dimensionless parameters. It was suggested that diamond, body-centered cubic (bcc) and other lattices can be obtained by controlling interactions between two particles. Starr et al. [74] have provided theoretical descriptions for equilibrium properties and the dynamics of DNA-linked nanoparticles with concepts from polymer physics, which was considered a successful way to describe novel self-assembly systems. Mirkin et al. [69] have also proposed a rule-based complementary contact model (CCM) to predict the crystal structures of DNA-grafted colloidal nanoparticles. Most recently, they have further constructed a simplified model to study the kinetics of the crystallization process, in which a given particle will transition between free, singly bound and doubly bound states [75]. Based on numerical solving of the thermodynamic equations, the variation of melting temperature and annealing window were predicted, suggesting that the model is useful in the design of future crystals.

From the computer simulation point of view, molecular dynamics (MD) simulation may be the most successful way to describe the dynamics of self-assembly. The first coarse-grained model for MD simulations was introduced by Sciortino et al. [76]. Later, this model was modified by Starr et al. [77]. In 2011, Travesset et al. [78] provided a new modified coarse-grained model to study the crystallization dynamics of DNA-coated nanoparticle systems. A key development of this model is that flanking beads are

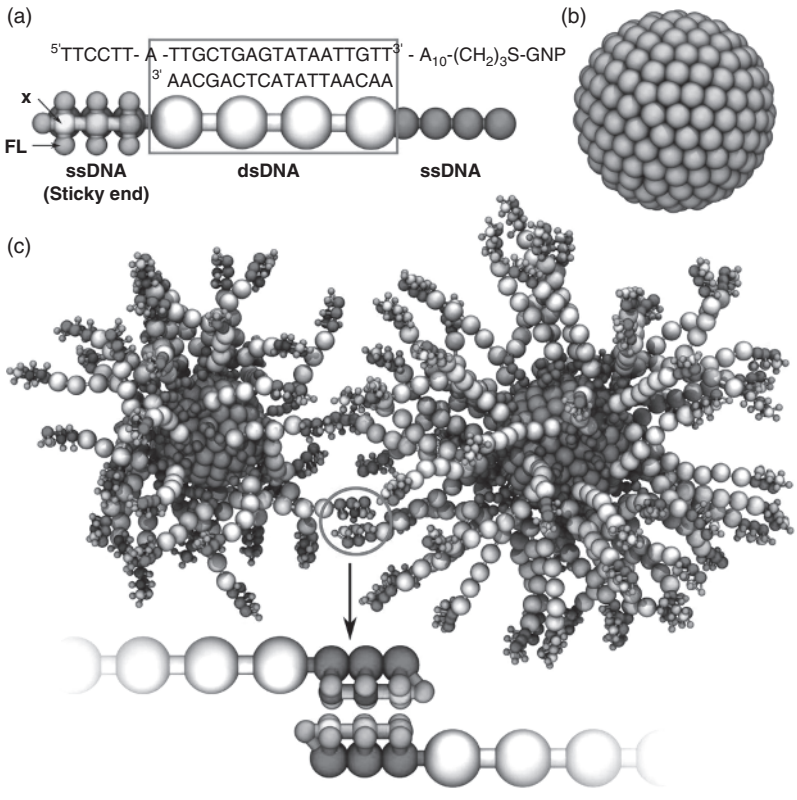

Figure 1.8 Cartoon of the coarse-grained model. (a) A model DNA chain for a sequence used in the experiments. The bead size for the dsDNA portion of the chain is σ, corresponding to a diameter of approximately 2 nm; the bead size for the ssDNA portion is 0.5σ, corresponding to an approximate diameter of 1 nm. (b) A model spherical GNP core. (c) An example of two SNA-GNPs: the particle on the left has an 8#nm gold core and 40 DNA chains; the particle on the right has a 10 nm core and 60 attached DNA chains. For more details, see Ref. [79], from which this figure is reproduced. Copyright permission from American Chemical Society (2012).

utilized to protect any base from binding to more than one complementary base. However, Travesset's model is limited to simulate the formation of many kinds of lattices that have been realized with dsDNA experimentally. To address this issue, de la Cruz et al. [79] proposed a new modified model to better describe these systems. It is to date the most detailed model that is able to capture the crystallization process of many nanoparticles. As seen in Figure 1.8, there are two main modifications in the model. First, the linker DNA chain contains both ssDNA and dsDNA and the dsDNA is modeled with a bead size two times larger than that of ssDNA. Second, the sizes of two nanoparticles, the number and the lengths of grafted DNA chains can be different. Their MD simulation results showed that binary superlattices of bcc, CsCl, AlB_2, Cr_3Si and Cs_6C_{60} can be assembled from binary mixtures of DNA-linked nanoparticles (Figure 1.9). The phase diagrams as a function of the particle size ratio and the DNA coverage ratios for three stoichiometric ratios (1:1, 1:2 and 1:3) were in accordance with experimental results. They also found that the crystallization process is accompanied

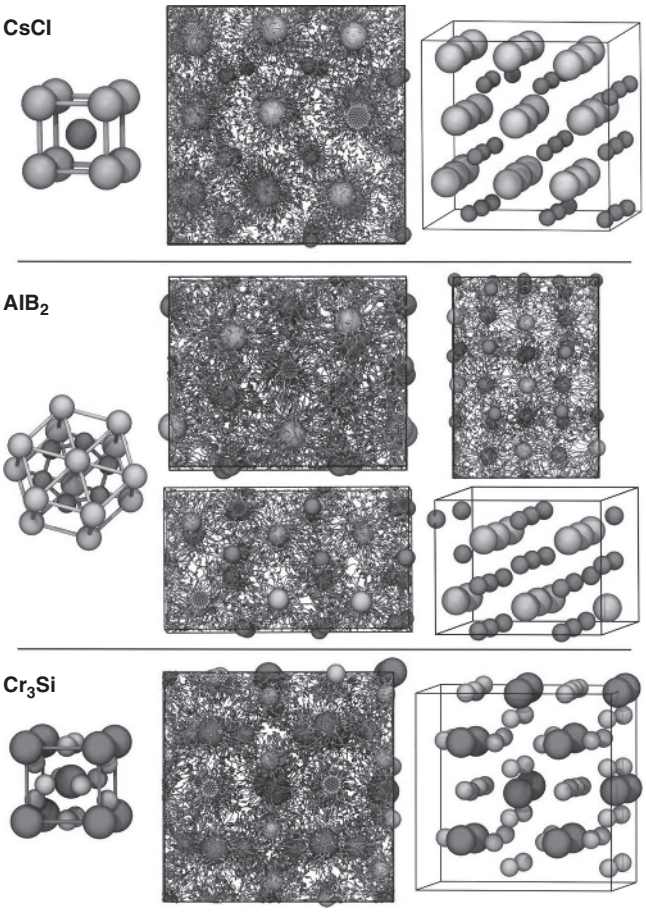

Figure 1.9 Snapshots of the crystal structures obtained from MD simulations. Left to right: The ideal crystal cell, a simulation snapshot after the system fully crystallized and the averaged positions of the SNA-GNPs. For more details, see Ref. [79], from which this figure is reproduced. Copyright permission from American Chemical Society (2012).

by a slight decrease of enthalpy. Furthermore, suitable linker sequences for future nanomaterial designs were proposed.

1.2.4 Self-Assembling Kinetics: Supracolloidal Reaction

The focus of nanoscience is gradually shifting from the synthesis of individual building blocks to the organization of larger nanostructures. The past decade has witnessed great progress in nanoparticle self-assembly, yet the quantitative prediction of the kinetics of their formation remains a challenge. In their pioneering research regarding this important topic, Kumacheva et al. [80, 81] reported on the marked similarity between the self-assembly of metal nanoparticles and reaction-controlled step-growth polymerization. Their results indicate that the kinetics and statistics of step-growth polymerization enable a quantitative prediction of the architecture of linear, branched

and cyclic self-assembled nanostructures; their aggregation numbers and size distribution; and the formation of structural isomers. The strong similarity of self-assembly of nanoparticles to polymerization reactions has also been identified in the kinetics of other colloidal systems [8, 83]. Based on this similarity, the molecular concepts of polymer chemistry can be applied to achieve controllable nanoparticle assembly. On the other hand, the ability to visualize nanoparticle assemblies and to exploit characterization tools used in nanoscience offers a unique way to study polymerization reactions. These works bridge the gap between polymerization reactions taking place at a molecular level and nanoparticle self-assembly occurring at a length scale two orders of magnitude larger.

In this context, Guo et al. [41] noted that the construction of supracolloidal helices through systematic computer simulations presents colloidal analogs of the molecular design to some supramolecules with ordered structures [83, 84]. The patchy particles act as multifunctional monomer units that "react" with each other, in a process analogous to supramolecular polymerization [83, 84]. The multi-patchy configuration significantly increases the sophistication of the kinetics and reaction pathway. Figure 1.10a shows the

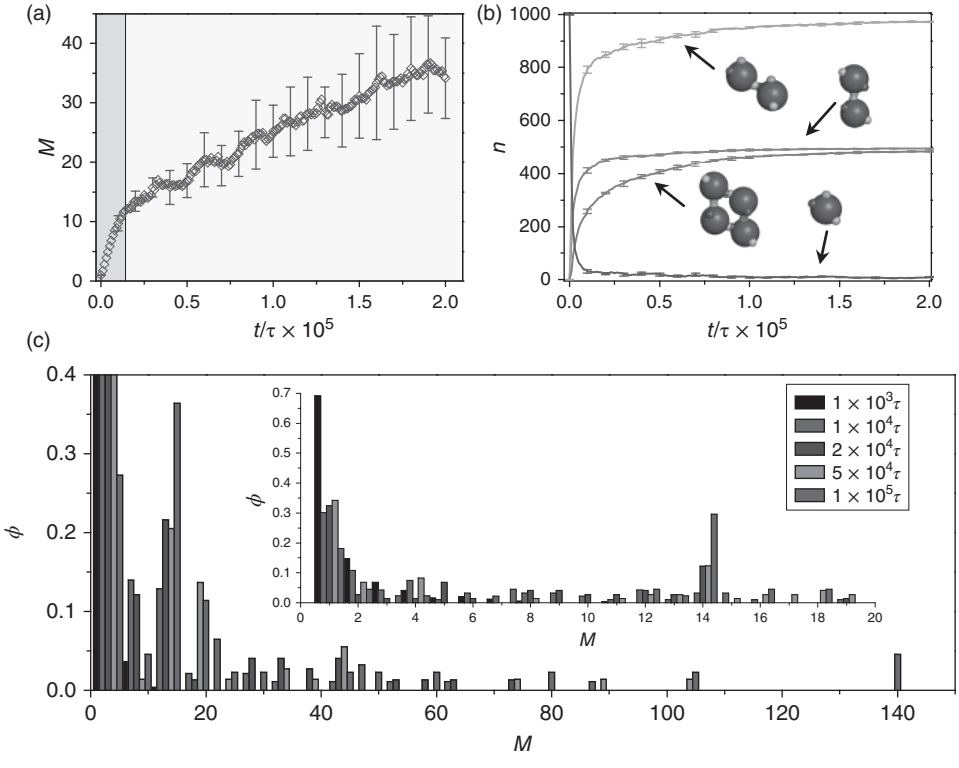

Figure 1.10 Kinetics in the self-assembling process of the helically supracolloidal structure. (a) The number-averaged degree of colloidal clusters as a function of self-assembling time *t*. (b) Variation in the number of patch groups in the course of self-assembly for species shown in inserts. (c) Number-averaged distributions of colloidal clusters at different times. Error bars in (a) and (b) indicate standard deviation. This figure is reproduced from Ref. 41. Copyright Permission from Nature Publishing Group (2014). *(See insert for color representation of the figure.)*.

time dependence of the average number of patchy particles in the supracolloidal chains, M, that resembles the number-averaged degree of polymerization. Interestingly, the $M-t$ plot can be divided into two regimes. In the first regime, M increases linearly with time, being characteristic of reaction-controlled step-growth polymerization. However, the linearity of the $M-t$ plot is relatively suppressed and the plot presents obvious fluctuation in the second regime.

To understand the kinetic mechanisms, they turned to a detailed analysis of the change in the concentrations of different species in the course of self-assembly [41]. Based on patchy interactions directed by their types, four representative species are concerned: individual patchy particle (IP), colloidal cluster linked by self-complementary patches (SP), colloidal cluster linked by a pair of complementary patches (PP) and the elementary colloidal cluster of perfect helix (EC) (Figure 1.10b). Figure 1.10b shows that the concentration of IP is extremely reduced at the initial stage owing to the formation of SP and PP. The complementary patches in SP and PP link each other spontaneously while the formation of EC with long-ranged patchy addition is relatively slow. Thus, the reactions of SP and PP dominate the kinetics in the first regime, resulting in the characteristic of reaction-controlled step-growth polymerization. In the second regime, however, the reaction of EC becomes the major effect, where sophisticated dynamical interconversion between clusters induces the obvious fluctuation in the kinetic plot. The distribution of colloidal clusters also becomes wider in the second regime, as demonstrated by Figure 1.10c. These finding may provide fundamental information for understanding the mechanisms of some reactions in supramolecule chemistry towards helically molecular architectures [83–85].

Acknowledgments

The authors thank Bojun Dong, Junshi Liang, Pengyu Chen, Ye Yang and Guolong Zhu for helpful discussions. This work is supported by the National Natural Science Foundation of China under grant nos. 51273105, 21422403 and 21174080, and the Ministry of Science and Technology of the People's Republic of China under grant no. 2016YFA0202500.

References

1. Whitesides, G. M.; Grzybowski, B. *Science* **2002**, *295*, 2418–2421.
2. Glotzer, S.C. *Science* **2004**, *306*, 419–420.
3. P. Ball, *The Self-Made Tapestry: Pattern Formation in Nature* (Oxford University Press, Oxford, **1999**).
4. Whitesides, G. M.; Boncheva, M. *Proc. Natl. Acad. Sci. U.S.A.* **2002**, *99*, 4769–4774.
5. Philip, D.; Stoddart, J. F. *Angew. Chem. Int. Ed.* **1996**, *35*, 1155–1196.
6. Frenkel, D. *Science* **2002**, *296*, 65–66.
7. Jones, M. R.; Mirkin, C. A. *Nature* **2012**, *491*, 42–43.
8. Wang, Y.; et al. *Nature* **2012**, *491*, 51–55.
9. Zhang, Z.; Glotzer, S. C. *Nano Lett.* **2004**, *4*, 1407–1413.
10. Glotzer, S. C.; Solomon, M. J. *Nat. Mater.* **2007**, *6*, 557–562.

11. Huang, M.; et al. *Science* **2015**, *348*, 424–428.
12. Gang, O.; Zhang, Y. *ACS Nano* **2011**, *5*, 8459–8465.
13. Walker, D. A.; Leitsch, E. K.; Nap, R. J.; Szleifer, I.; Grzybowski, B. *Nat. Nanotech.* **2013**, *8*, 676–681.
14. Frenkel, D. *Nat. Mater.* **2015**, *14*, 9–12.
15. Cates, M. E. *Nat. Mater.* **2013**, *12*, 179–180.
16. Balazs, A. C.; Emrick, T.; Russell, T. P. *Science* **2006**, *314*, 1107–1110.
17. Yan, L. T.; Xie, X. M. *Prog. Polym. Sci.* **2013**, *38*, 369–406.
18. Grzelczak, M.; Vermant, J.; Furst, E. M.; Liz-Marzan, L. M. *ACS Nano* **2010**, *4*, 3591–3605.
19. Schatz, G. C. *Proc. Natl. Acad. Sci. U.S.A.* **2007**, *104*, 85–92.
20. Service, R. F. *Science* **2012**, *335*, 1434–1435.
21. Karttunen, M.; Vattulainen, I.; Lukkarinen, A. *Novel Methods in Soft Matter Simulations* (Springer, Berlin, **2004**).
22. Burda, C.; Chen, X.; Narayanan, R.; El-sayed, M. *Chem. Rev.* **2005**, *105*, 1025–1102.
23. Frenkel, D. *Physica A* **2002**, *313*, 1–31.
24. Gudiksen, M. S.; Lauhon, L. J.; Wang, J.; Smith, D. C.; Lieber, C. M. *Nature* **2002**, *415*, 617–620.
25. Veerman, J. A. C.; Frenkel, D. *Phys. Rev. A* **1992**, *45*, 5632–5648.
26. John, B. S.; Escobedo, F. A. *J. Chem. Phys.* **2008**, *128*, 044909.
27. Yin, J. S.; Wang, Z. L. *Phys. Rev. Lett.* **1997**, *79*, 2570–2573.
28. Maeda, H.; Maeda, Y. *Phys. Rev. Lett.* **2003**, *90*, 018303.
29. Haji-Akbari, A.; et al. *Nature* **2009**, *462*, 773–777.
30. Agarwal, U.; Escobedo, F. A. *Nat. Mater.* **2011**, *10*, 230–235.
31. Damasceno, P. F.; Engel, M.; Glotzer, S. C. *Science* **2012**, *337*, 453–457.
32. Ramano, F.; Sciortino, F. *Nature Comm.* **2012**, *3*, 975–980.
33. Morgan, J. W. R.; Chakrabarti, D.; Dorsaz, N.; Wales, D. J. *ACS Nano* **2013**, *7*, 1246–1256.
34. Harris, A. B.; Kamien, R. D.; Lubensky, T. C. *Rev. Mod. Phys.* **1999**, *71*, 1745–1757.
35. Gansel, J. K. et al. *Science* **2009**, *325*, 1513–1515.
36. Inoue, Y.; Ramamurthy, V. *Chiral Photochemistry* (Marcel Dekker Press, New York, 2004).
37. Soukoulis, C. M.; Wegener, M. *Nature Photon.* **2011**, *5*, 523–530.
38. Kuzyk, A.; et al. *Nature* **2012**, *483*, 311–314.
39. Song, C.; et al. *Nano Lett.* **2013**, *13*, 3256–3261.
40. Fan, Z.; Govorov, A. O. *Nano Lett.* **2010**, *10*, 2580–2587.
41. Guo, R.; Mao, J.; Xie, X. M.; Yan, L. T. *Sci. Rep.* **2014**, *4*, 7021.
42. Szleifer, I. *Nat. Mater.* **2013**, *12*, 693–694.
43. Sheiko, S. S.; Zhou, J.; Arnold, J.; Neugebauer, D.; Matyjaszewski, K.; Tsitsilianis, C.; Tsukruk, V.; Carrillo, J. M. Y.; Dobrynin, A. V.; Rubinstein, M. *Nat. Mater.* **2013**, *12*, 735–740.
44. De Nijs, B.; Dussi, S.; Smallenburg, F.; Meeldijk, J. D.; Groenendijk, D. J.; Filion, L.; Imhof, A.; van Bladderen, A.; Dijkstra, M. *Nat. Mater.* **2015**, *14*, 56–60.
45. Zhang, D.; Carignano, M. A.; Sleifer, I. *Phys. Rev. Lett.* **2006**, *96*, 028701.
46. Alder, B. J.; Wainwright, T. E. *J. Chem. Phys.* **1957**, *27*, 1208–1209.
47. Pusey, P. N.; Van Megen, W. *Nature* **1986**, *320*, 340–342.
48. Chen, Q.; Bae, S.; Granick, S. *Nature* **2011**, *469*, 381–384.

49. Mao, X.; Chen, Q.; Granick, S. *Nature Mater.* **2013**, *12*, 217–222.
50. de Graaf, J.; van Roij, R.; Dijkstra, M. *Phys. Rev. Lett.* **2011**, *107*, 155501.
51. Ni, R.; Gantapara, A. P.; de Graaf, J.; van Roij, R.; Dijkstra, M. *Soft Matter* **2012**, *8*, 8826–8834.
52. van Anders, G.; Klotsa, D.; Ahmed, N. K.; Engel, M.; Glotzer, S. C. *Proc. Natl Acad. Sci. USA* **2014**, *111*, E4812–E4821.
53. Kao, J.; Thorkelsson, K.; Bai, P.; Rancatore, B. J.; Xu, T. *Chem. Soc. Rev.* **2013**, *42*, 2654–2678.
54. Bockstaller, M. R.; Thomas, E. L. *Phys. Rev. Lett.* **2004**, *93*, 166106.
55. Lin Y.; Böker, A.; He, J.; Sill, K.; Xiang, H.; Abetz, C.; Li, X.; Emrick, T.; Long, S.; Wang, Q.; Balazs, A. C.; Russell, T. P. *Nature* **2005**, *434*, 55–59.
56. Thompson, R. B.; Ginzburg, V. V.; Matsen, M. W.; Balazs, A. C. *Science* **2001**, *292*, 2469–2472.
57. Yan, L. T.; Popp, N.; Ghosh, S. K.; Böker, A. *ACS Nano* **2010**, *4*, 913–920.
58. Dong, B.; Guo, R.; Yan, L. T. *Macromolecules* **2014**, *47*, 4369–4379.
59. Dong, B.; Huang, Z.; Chen, H.; Yan, L. T. *Macromolecules* **2015**, *48*, 5385–5393.
60. Liu, Z.; Guo, R.; Xu, G.; Huang, Z.; Yan, L. T. *Nano Lett.* **2014**, *14*, 6910–6916.
61. Huang, Z.; Lu, C.; Dong, B.; Xu, G.; Ji, C.; Zhao, K.; Yan, L. T. *Nanoscale* **2016**, *8*, 1024–1032.
62. Cademartiri, L.; Bishop, K. J. M. *Nat. Mater.* **2015**, *14*, 2–9.
63. Lehn, J. M. *Angew. Chem. Int. Ed.* **2013**, *52*, 2836–2850.
64. Cartwright, J. H. E.; Mackay, A. L. *Phil. Trans. R. Soc. A* **2012**, *370*, 2807–2822.
65. Soloveichik, D.; Winfree, E. *SIAM J. Comput.* **2007**, *36*, 1544–1569.
66. Mirkin, C. A.; Letsinger, R. L.; Mucic, R. C.; Storhoff, J. J. *Nature* **1996**, *382*, 607–609.
67. Alivisatos, A.; et al. *Nature* **1996**, *382*, 609–611.
68. Biancaniello, P.; Kim, A.; Crocker, J. *Phys. Rev. Lett.* **2005**, *94*, 58302.
69. Macfarlane, R. J.; et al. *Science* **2011**, *334*, 204–208.
70. Feng, L.; Dreyfus, R.; Sha, R. J.; Seeman, N. C.; Chaikin, P. M. *Adv. Mater.* **2013**, *25*, 2779–2783.
71. Yan, W.; et al. *J. Am. Chem. Soc.* **2012**, *134*, 15114–15121.
72. Jones, M. R.; et al. *Nat. Mater.* **2010**, *9*, 913–917.
73. Tkachenko, A. V. *Phys. Rev. Lett.* **2002**, *89*, 148303.
74. Hsu, C. W.; Sciortino, F.; Starr, F. W. *Phys. Rev. Lett.* **2010**, *105*, 55502.
75. Macfarlane, R. J.; Thaner, R. V.; Brown, K. A.; Zhang, J.; Lee, B.; Nguyen, S. T.; Mirkin, C. A. *Proc. Natl. Acad. Sci. USA* **2014**, *111*, 14995–15000.
76. Starr, F. W.; Sciortino, F. *J. Phys.: Condens. Matter* **2006**, *18*, L347–L353.
77. Vargas Lara, F.; Starr, F. W. *Soft Matter* **2011**, *7*, 2085–2096.
78. Knorowski, C.; Burleigh, S.; Travesset, A. *Phys. Rev. Lett.* **2011**, *106*, 21550.
79. Li, T.; Sknepnek, R.; Macfarlane, R. J.; Mirkin, C. A.; de la Cruz, M. O. *Nano Lett.* **2012**, *12*, 2509–2514.
80. Liu, K.; et al. *Science* **2010**, *329*, 197–200.
81. Klinkovaa, A.; Thérien-Aubina, H.; Choueiria, R. M.; Rubinsteinb, M.; Kumacheva, E. *Proc. Natl. Acad. Sci. USA* **2013**, *110*, 18775–18779.
82. Chen, Q.; Whitmer, J. K.; Jiang, S.; Bae, S. C.; Luijten, E.; Granick, S. *Science* **2011**, *331*, 199–202.

83. van Gorp, J. J.; Vekemans, J.; Meijer, E. W. *J. Am. Chem. Soc.* **2002**, *124*, 14759–14769.
84. Kim, H. J.; Zin, W. C.; Lee, M. *J. Am. Chem. Soc.* **2004**, *126*, 7009–7014.
85. Ho, R. M.; Chiang, Y. W.; Lin, S. C.; Chen, C. K. *Prog. Polym. Sci.* **2011**, *36*, 376–453.